Dyes and Pigments 184 (2021) 108868

Contents lists available at ScienceDirect

Dyes and Pigments

journal homepage: http://www.elsevier.com/locate/dyepig

Phenothiazine and diphenylsulfone-based donor–acceptor π-systems exhibiting remarkable mechanofluorochromism

Hongke Zhou [a], Qian Huang [a], Xingliang Liu [a], Defang Xu [b,*], Weidong Zhang [a], Shengjie Fu [a], Xiucun Feng [a], Zhan Zhang [a]

[a] School of Chemical Engineering, Qinghai University, Xining, 810016, China
[b] State Key Laboratory of Plateau Ecology and Agriculture, Qinghai University, Xining, 810016, China

ARTICLE INFO

Keywords:
Phenothiazine
Diphenylsulfone
Intramolecular charge transfer
Mechanofluorochromism

ABSTRACT

Two donor–acceptor luminophores **PTZ-DPS** and **BPTZ-DPS**, which are constructed by electron-donor phenothiazine and electron-acceptor diphenylsulfone moiety, are designed and synthesized. Through the effective combination of phenothiazine and diphenylsulfone unit, **PTZ-DPS** and **BPTZ-DPS** molecules adopt twisted molecular conformation, unique intramolecular charge transfer (ICT) behavior and intense fluorescence in both solution and solid state. The solid-state luminescence efficiencies of the two luminophores reach 32.84% and 39.69%, respectively. It is particularly noteworthy that both **PTZ-DPS** and **BPTZ-DPS** exhibit switchable mechanofluorochromism with high contrast. Upon external force stimulation, the fluorescence colors of the **PTZ-DPS** and **BPTZ-DPS** solid powders that change dramatically from initial bright green and yellow to orange, respectively, are observed. Meanwhile, the emission bands red shift from 499 nm to 564 nm–589 nm and 592 nm, respectively, suggesting the large spectral red shifts of 90 nm and 28 nm. Moreover, the mechanofluorochromic (MFC) behavior of **PTZ-DPS** and **BPTZ-DPS** also show good reversibility when fume the ground powders by DCM vapor. PXRD and spectral data suggest that the phase transition between crystalline to amorphous states is responsible for MFC behavior of **PTZ-DPS** and **BPTZ-DPS,** and the red-shift in the PL spectrum upon grinding originates from the planarization of the molecular conformation and subsequent planar intramolecular charge transfer (PICT).

1. Introduction

Mechanofluorochromic (MFC) material [1] is an important kind of intelligent fluorescent material which can change the emission colors or intensities of solid-state fluorescence under the external force stimulation, such as shearing, pressing, grinding, deformation, etc.). Recently, the design and synthesis of MFC materials have aroused increased interest due to their fundamental importance and potential applications in information storages [2], mechano-sensors [3], security inks [4], and anti-counterfeiting materials [5]. In principle, there are two effective ways, the chemical and physical methods, to achieve the tuning of the solid-state fluorescence of conjugated organic materials [6]. The chemical method involves solid-state chemical reactions, which not only cause changes in the chemical structure of molecules, but also have some shortcomings including insufficient conversion, irreversibility as well as loss of luminescence of reactants. In contrast, the physical method shows good prospects and advantages. That is because this method only involves the changes in the molecular packing mode, but does not alter the chemical structure of molecules. And thus control of molecular packing becomes a promising strategy to tune the optical properties of fluorophores due to the strong dependence of solid-state optical properties on the molecular packing arrangements. Therefore, various types of MFC molecules, including the derivatives of tetraphenylethene [7], carbazole [8], 3,6-bis(aryl)-1,4-diketo-pyrrolo[3,4-*c*]pyrroles (DPPs) [9], 9,10-divinylanthracene [10] and oligo(*p*-phenylene vinylene) [11], as well as some organoboron complexes [12,13], which can change their molecular stacking modes, have been designed and prepared to date. Due to the close relationships between the molecular stacking modes and the molecular conformations as well as the intermolecular interactions, the desired packing modes can be gained by properly modifying the molecular structures of specific fluorophores. The change of high contrast fluorescence color before and after stimulation by external force and good solid-state luminescence efficiency are two important indexes to evaluate MFC materials. In general, for an organic

---

* Corresponding author.
E-mail address: xudefang123@163.com (D. Xu).

https://doi.org/10.1016/j.dyepig.2020.108868
Received 14 August 2020; Received in revised form 12 September 2020; Accepted 15 September 2020

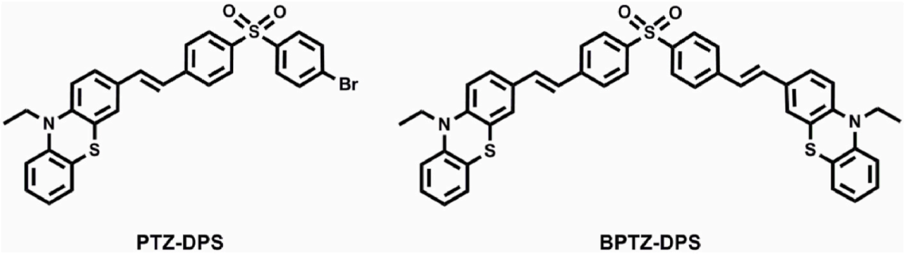

Scheme 1. The molecular structures of **PTZ-DPS** and **BPTZ-DPS**.

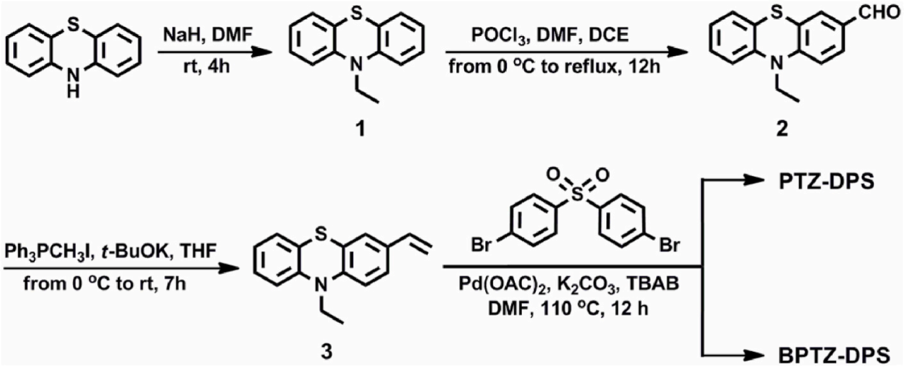

Scheme 2. Synthetic routes of **PTZ-DPS** and **BPTZ-DPS**.

luminophores, the highly twisted molecular conformation can effectively inhibit intermolecular interactions and strong π-π stacking in the aggregate state to a certain extent, which avoids the appearance of the infamous aggregation-induced quenching (ACQ) effect [14] that are commonly seen in organic fluorescent molecules and thus results in solid-state fluorescence [15]. Not only that, this twisted molecular conformation can also promote the dye molecules to form loose packing in the crystalline state, which are conducive to the changes of stacking modes under the external force. Therefore, much effort has been devoted to design and prepare organic molecules with twisted molecular conformations, and many MFC fluorophores have been reported [16]. However, in fact, there are still some disputes about the mechanism of MFC behavior at present. The design rules reported in the literatures are only applicable to specific molecules. So there is no general design strategy for the design of MFC molecules. It is difficult to determine whether the designed molecules have MFC properties. Therefore, it is urgent to design and prepare new MFC molecules to understand the underlying mechanism of MFC phenomenon in depth, so as to establish the internal relationship between molecular structure and performance.

Due to fascinating optical properties and potential applications range from organic light-emitting diodes (OLED) to chemosensors [17], electron donor-acceptor (D–A) structured π-systems have been the subject of intense research. More importantly, the electronic structures and thus optoelectronic properties of this kind of luminogens can be facilely modulated by tuning the electron donor and/or acceptor strengths. Current researches show that D–A molecules bearing obvious ICT characteristics and twisted molecular conformation exhibit ideal solid-state luminescence properties and MFC behavior in vividly contrasting colors [16,18]. Herein, we designed and synthesized two D–A structured molecules **PTZ-DPS** and **BPTZ-DPS** (Scheme 1), in which phenothiazine and diphenylsulfone unit are selected as electron-donating and electron-accepting segments, respectively. Through this reasonable combination of bowl-shaped phenothiazine and diphenylsulfone, the two compounds possessing the twisted molecular conformation are obtained. As expected, **PTZ-DPS** and **BPTZ-DPS** show obvious ICT effect, intense fluorescence in both solution and solid state, and high contrast mechanochromic luminescence.

2. Experimental section

2.1. Materials and measurements

General. The ^{1}H and^{13}C NMR spectra were obtained with a Bruker-Avance III (400 MHz and 100 MHz) spectrometer by using $CDCl_3$ as the solvent and tetramethylsilane (TMS) as the internal standard. The high-resolution mass spectrometry (HRMS) was carried out using a matrix-assisted laser desorption ionization time-of-flight mass spectrometry (MALDI-TOF MS, Performance (Shimadzu, Japan)). The IR spectra were measured with a Nicolet-360 FTIR spectrometer by incorporation of samples in KBr disks. Elemental analyses for C, H, N were carried out on a Perkin-Elmer 240C elemental analyzer. The UV–vis absorption spectra of solution/solid samples were recorded on a Shimadzu UV-2550 spectrophotometer and fluorescence spectra on a Cary Eclipse fluorescence spectrophotometer. Quantum yields and time-resolved fluorescence decay profiles of the solid samples were recorded on an Edinburgh FLS920 steady state and time-resolved fluorescence spectrometer. Cyclic voltammetry was performed at room temperature in a three electrode cell by using a Metrohm Autolab PGSTAT204 Electrochemical Workstation with a scan rate at 50 mV s^{-1}. The working electrode was a platinum button, the counter electrode was a platinum wire, and Ag/Ag^+ was used as reference electrode. $(C_4H_9)_4NBF_4$ was used as the supporting electrolyte in dry DCM. Powder X-Ray diffraction (PXRD) patterns were collected by a Bruker D8 Focus Powder X-ray diffraction instrument. The HOMO/LUMO orbitals of target compounds **PTZ-DPS** and **BPTZ-DPS** were calculated at the B3LYP/6-31G (d, p) level with the Gaussian 09W program package.

Mechanofluorochromic and stimuli-recovering experiments

Grinding experiment: The as-prepared solid powders of **PTZ-DPS** and **BPTZ-DPS** were put into a mortar and then ground with a pestle at room temperature. Solvent-fuming experiment: the ground samples were suspended above the solvent level in a sealed DCM containing beaker and then were exposed to the vapor for 30 s at room temperature.

Materials. DMF was was dried over CaH and distilled under reduced pressure before use. THF was dried and purified by distilling it from sodium and benzophenone in an atmosphere of dry nitrogen. The other

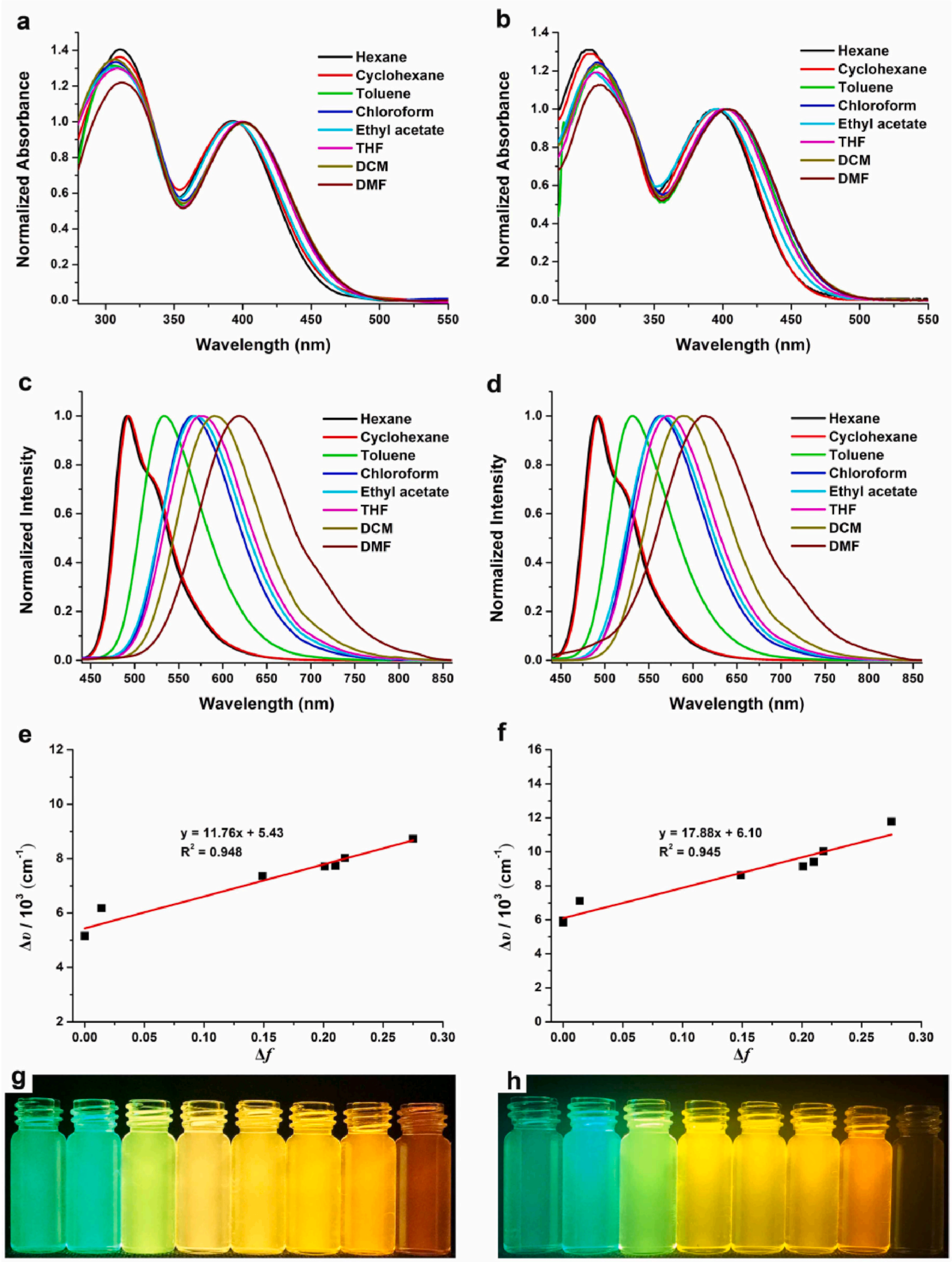

Fig. 1. Normalized UV–vis absorption spectra (a: **PTZ-DPS;** b: **BPTZ-DPS**) and normalized PL spectra (c: **PTZ-DPS;** d: **BPTZ-DPS**) in solvents with different polarities (1.0×10^{-5} mol L^{-1}, $\lambda_{ex} = 410$ nm); Plots of Stokes shift ($\Delta \upsilon$) vs solvent polarity parameter (Δf) (e: **PTZ-DPS;** f: **BPTZ-DPS**); Photos in various solvents under 365 nm UV light (g: **PTZ-DPS;** h: **BPTZ-DPS**. From left to right: Hexane, Cyclohexane, Toluene, Chloroform, Ethyl acetate, THF, DCM, DMF).

reagents and solvents were used as received from commercial suppliers without further purification.

2.2. Synthesis

2.2.1. (E)-3-(4-((4-bromophenyl)sulfonyl)styryl)-10-ethyl-10H-phenothiazine (PTZ-DPS)

Compound **3** (1.34 g, 5.29 mmol) and 4,4′-sulfonylbis (bromobenzene) (1.99 g, 5.29 mmol) were dissolved in dry DMF, and then anhydrous potassium carbonate (2.20 g, 15.92 mmol), tetrabutylammonium bromide (2.50 g, 7.76 mmol) and Pd(OAc)$_2$ (30 mg, 0.134 mmol) was added. The mixture was heated to reflux for 6 h under an atmosphere of nitrogen. After being cooled to room temperature, the mixture was poured into 400 mL water with stirring and then extracted three times with CH$_2$Cl$_2$. The combined organic phases were washed with brine, and then dried over anhydrous Na$_2$SO$_4$. The solvent was removed and the crude product was purified on silica gel column chromatography by using petroleum ether/CH$_2$Cl$_2$ (v/v = 1/2) as eluent, giving a light yellow-green solid (1.90 g). Yield 65%. ^{1}H NMR (400 MHz, CDCl$_3$) δ 7.88 (d, J = 8.4 Hz, 2H), 7.81 (d, J = 8.8 Hz, 2H), 7.65 (d, J = 8.4 Hz, 2H), 7.57 (d, J = 8.0 Hz, 2H), 7.30-7.26 (m, 2H), 7.18-7.06 (m, 3H), 6.94-6.86 (m, 4H), 3.96-3.94 (m, 2H), 1.44 (t, J = 6.8 Hz, J = 6.8 Hz, 3H) (Figs. S3 and S4); ^{13}C NMR (100 MHz, CDCl$_3$) δ 142.83, 141.01, 138.88, 132.57, 131.41, 131.37, 130.70, 129.07, 128.29, 128.14, 127.38, 126.88, 126.52, 125.18, 125.15, 125.11, 125.09, 124.87, 124.73, 124.66, 124.61, 124.52, 122.72, 122.67, 115.14, 114.96, 41.97, 13.01 (Fig. S5); HRMS (MALDI-TOF) m/z: [M]$^+$ Calcd for C$_{28}$H$_{22}$BrNO$_2$S$_2$ 547.0275; Found 547.0266 (Fig. S6); IR (KBr, cm^{-1}): 538、689、717、767、941、990、1075、1218、1300、1345、1410、1530、1597、1661. Anal. Calcd (%) for C$_{28}$H$_{22}$BrNO$_2$S$_2$: C 61.31, H 4.04, N 2.55; Found: C 61.12, H 4.25, N 2.44.

2.2.2. 3,3'-((1E,1′E)-(sulfonylbis(4,1-phenylene))bis(ethene-2,1-diyl))bis (10-ethyl-10H-phenothiazine) (BPTZ-DPS)

BPTZ-DPS was synthesized from compound **3** (2.96 g, 11.70 mmol), 4,4′-sulfonylbis(bromobenzene) (2.00 g, 5.32 mmol) anhydrous potassium carbonate (4.40 g, 31.84 mmol), tetrabutylammonium bromide (5.00 g, 15.51 mmol) and Pd(OAc)$_2$ (40 mg, 0.178 mmol) following the same procedure as that of **PTZ-DPS,** affording a bright yellow solid (3.26 g). Yield 85%. ^{1}H NMR (400 MHz, CDCl$_3$) δ 7.90 (d, J = 8.4 Hz, 4H), 7.56 (d, J = 8.4 Hz, 4H), 7.27 (t, J = 6.8 Hz, J = 6.4 Hz, 4H), 7.18-7.05 (m, 6H), 6.95-6.84 (m, 8H), 3.94 (s, 4H), 1.43 (t, J = 6.8 Hz, J = 6.8 Hz, 6H) (Figs. S7 and S8); ^{13}C NMR (100 MHz, CDCl$_3$) δ 145.00, 144.17, 142.40, 139.69, 131.10, 130.85, 130.82, 128.03, 127.38, 126.78, 126.47, 125.16, 124.82, 124.74, 124.70, 124.68, 123.60, 122.67, 115.18, 115.02, 53.50, 42.04, 12.92 (Fig. S9); HRMS (MALDI-TOF) m/z: [M]$^+$ Calcd for C$_{44}$H$_{36}$N$_2$O$_2$S$_3$ 720.1939; Found 720.1929 (Fig. S10); IR (KBr, cm^{-1}): 534、652、694、743、913、984、1078、1190、1358、1402、1565、1602、1659. Anal. Calcd. (%) for C$_{44}$H$_{36}$N$_2$O$_2$S$_3$: C 73.30, H 5.03, N 3.89; Found: C 73.11, H 5.23, N 4.06.

3. Result and discussion

*3.1. Synthesis of **PTZ-DPS** and **BPTZ-DPS***

The synthesis of **PTZ-DPS** and **BPTZ-DPS** is showed in Scheme 2. The general route to **PTZ-DPS** and **BPTZ-DPS** started from phenothiazine. Firstly, the 3-aldehyde phenothiazine possessing an ethyl was obtained by Vilsmeier reactions of N-ethyl-substituted phenothiazine [19], which was synthesized by the alkylation of phenothiazine by using bromoethane and NaH in DMF [19]. Then, the important precursor **3** was synthesized via Wittig reaction between methyltriphenylphosphoniumiodine (Ph$_3$PCH$_3$I) and compound **2** [20]. Finally, Heck reaction [21] catalyzed by Pd(OAC)$_2$ was carried out between the precursor **3** with 4,4′-sulfonylbis(bromobenzene) to give the target compounds **PTZ-DPS** (1.0 equiv of **3**) and **BPTZ-DPS** (2.2 equiv of **3**) with good yields of 65% and 85%, respectively. All the intermediates and the target compounds were purified by column chromatography, and ^{1}H NMR, ^{13}C NMR, the high-resolution mass spectrometry (HRMS), and elemental analysis (C, H and N) were employed to confirm the chemical structures of the new compounds. In organic solvents (CHCl$_3$, CH$_2$Cl$_2$, THF, benzene and toluene), **PTZ-DPS** and **BPTZ-DPS** exhibit good solubility, but they show poor solubility in alcohols (methanol and ethanol) and aliphatic hydrocarbon solvents (hexane and cyclohexane).

Table 1
UVvis absorption and fluorescence Properties of **PTZ-DPS** and **BPTZ-DPS** in different solvents.

Compound	Solvent	λ_{abs}/nm (ε/M^{-1} cm^{-1})	λ_{em}/ nm	$\Delta\upsilon_{st}$[a]/ cm^{-1}	Φ_f[b]
PTZ-DPS	hexane	312 (20200), 392 (14500)	491	5143	0.35
	cyclohexane	310 (21100), 393 (15100)	493	5161	0.26
	toluene	309 (19800), 401 (15000)	533	6176	0.25
	chloroform	308 (18900), 400 (14000)	567	7363	0.25
	ethyl acetate	307 (22500), 395 (17400)	568	7711	0.21
	THF	307 (23900), 399 (18400)	577	7731	0.20
	DCM	306 (23200), 401 (17300)	591	8017	0.17
	DMF	312 (21200), 401 (17200)	617	8730	0.05
BPTZ-DPS	hexane	306 (51700), 394 (40100)	491	5014	0.34
	cyclohexane	306 (52000), 395 (40400)	493	5032	0.26
	toluene	311 (50900), 404 (41600)	532	5955	0.20
	chloroform	309 (53100), 403 (42600)	563	7052	0.18
	ethyl acetate	309 (52200), 396 (43900)	566	7584	0.18
	THF	308 (53700), 402 (45100)	574	7454	0.17
	DCM	309 (53600), 404 (43400)	589	7775	0.14
	DMF	310 (50000), 405 (44500)	614	8405	< 0.01

[a] $\Delta\upsilon_{st} = \upsilon_{abs}$-$\upsilon_{em}$.
[b] The fluorescence quantum yield (Φ_f) was measured using quinine sulfate as a standard (Φ_f = 0.546 in 0.5 mol L^{-1} H$_2$SO$_4$).

*3.2. Photophysical properties of **PTZ-DPS** and **BPTZ-DPS** in solutions*

In the molecular framework of compounds **PTZ-DPS** and **BPTZ-DPS**, there are typical electron donor phenothiazine and electron acceptor diphenylsulfone units [22]. The combination of these two units is advantageous to the occurrence of intramolecular charge transfer (ICT) process. Generally, the photophysical properties of D–A molecules in solution are strongly dependent on the polarity of solvents. Therefore, the optical properties of **PTZ-DPS** and **BPTZ-DPS** were investigated by UV–visible absorption (Fig. 1a and b) and photoluminescence (PL) spectra (Fig. 1c and d) in varying solvents. As depicted in Fig. 1a and b, both compounds possess very similar absorption spectra showing two intense major absorption bands in the solvents of different polarities with shorter/longer-wavelength absorptions of ca. 310/395 and ca. 310/400 nm, respectively. The former band can be attributed to the π–π* transitions, while the latter comes from the ICT transitions between electron donor phenothiazine and electron acceptor diphenylsulfone segments. This conclusion can be confirmed by the solvent-dependent absorption spectra [23]. In hexane, the longer-wavelength absorption bands of **PTZ-DPS** and **BPTZ-DPS** appear at 392 and 394 nm, respectively. With the increase of solvent polarity, they show a slight red shift trend and reach 401 and 405 nm in DMF. In contrast, the PL spectra of **PTZ-DPS** and **BPTZ-DPS** are strongly affected by the polarities of the solvents. As shown in Fig. 1c and d, **PTZ-DPS** and **BPTZ-DPS** both exhibit a significant red-shift and broad spectra when the solvent polarity increased from hexane to DMF, respectively. For example, in hexane, the emission peaks of **PTZ-DPS** and **BPTZ-DPS** both appear at 491 nm, with the increase of solvent polarity, they red shift to 567 and 563 nm in chloroform, and finally reach 617 and 614 nm in DMF, respectively, indicating an obvious bathochromic effect.

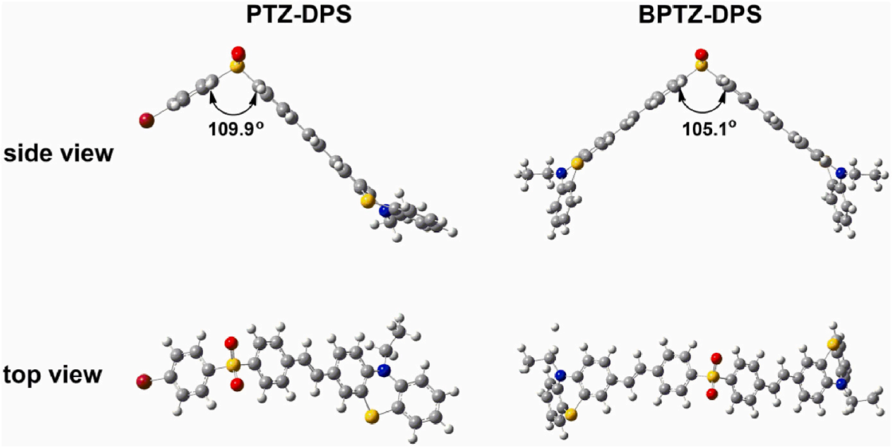

Fig. 2. Optimized geometry for **PTZ-DPS** and **BPTZ-DPS** using Gaussian 09 programme at the B3LYP/6-31G(d,p) level.

Accordingly, the fluorescence color of **PTZ-DPS** and **BPTZ-DPS** solutions changes from blue-green to yellow, and finally to orange red (Fig. 1g and h). The above results directly point to the occurrence of ICT between the donor and the acceptor [23], which would enhance the dipole-dipole interaction between the dye and the solvent molecules, and thus decreases the excited state energy as a result of the solvent relaxation. In addition, it should be noted that both compounds exhibit well-defined fluorescence bands in nonpolar solvents, indicating the existence of two separated close-lying excited states. We believe that the emission of **PTZ-DPS** and **BPTZ-DPS** in hexane and cyclohexane originates from the locally excited (LE) state [24]. However, in polar solvents, their spectral bands become structureless and broader. This further demonstrates the occurrence of the extensive ICT in polar environment. The Stokes shifts ($\Delta\upsilon$) of **PTZ-DPS** and **BPTZ-DPS** in varying solvents are calculated and collected in Table 1. We can see clearly that the Stokes shifts of the two compounds increase from 5143 to 5014 cm^{-1} in hexane to 8730 and 8405 cm^{-1} in DMF, respectively. The solvatochromic behavior of the two compounds was quantitatively described by the Lippert−Mataga equation [25].

$$\Delta\upsilon = \upsilon_a - \upsilon_e = \frac{2\Delta f}{hca^3}(\mu_E - \mu_G)^2 + \text{constant} \tag{1}$$

where υ_a and υ_e represent the maximum absorbance and emission wavenumbers, μ_G and μ_E are the dipole moments in the ground and excited states, and h, c, a, and n are the Planck constant, the speed of light, the Onsager solvent cavity radius, and the refractive index of the solvent, respectively.

The orientational polarizability Δf that is described in eq (2) is chosen as the measure of polarity.

$$\Delta f = \frac{\varepsilon - 1}{2\varepsilon + 1} - \frac{n^2 - 1}{2n^2 + 1} \tag{2}$$

where ε and n are the static dielectric constant and the optical refractive index of the solvent, respectively.

As shown in Fig. e, f, the linear relationship between $\Delta\nu$ and Δf and the large slope of $\Delta\upsilon$ and Δf curves (**PTZ-DPS**: 11760 cm^{-1}; **BPTZ-DPS**: 17880 cm^{-1}) suggest that the dipole moment of ICT excited state is larger than that of ground state because of the substantial charge redistribution, which may be stemmed from the relaxation of the initially formed Franck−Condon excited state. At the same time, the nearly equal slope of $\Delta\upsilon$ and Δf curves also means that the ICT degree of the two compounds is similar. Moreover, we measured the fluorescence quantum yields (Φ_f) of **PTZ-DPS** and **BPTZ-DPS** in different solvents by using quinine sulfate ($\Phi_f = 0.546$, 0.5 mol L^{-1} H_2SO_4) as the standard, which were collected in Table 1. Both the two compounds exhibit a positive solvatokinetic effect. When the solvent polarity increases from hexane to DMF, the Φ_f of **PTZ-DPS** and **BPTZ-DPS** decreases from 0.35 to 0.34 in hexane to 0.25 and 0.18 in chloroform, and in DMF it is finally reduced to 0.05 and $<$ 0.01, respectively, which shows a significant downward trend in response to a positive solvatokinetic effect [8a]. It is believed that the relatively strong fluorescence of **PTZ-DPS** and **BPTZ-DPS** in nonpolar solvents originates from restricted ICT

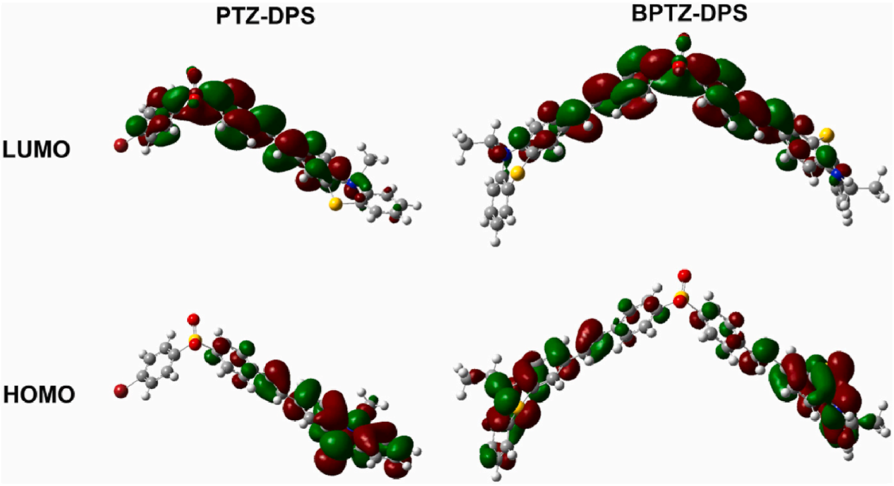

Fig. 3. Calculated spatial distributions of HOMO and LUMO levels for **PTZ-DPS** and **BPTZ-DPS** using Gaussian 09 programme at the B3LYP/6-31G(d,p) level.

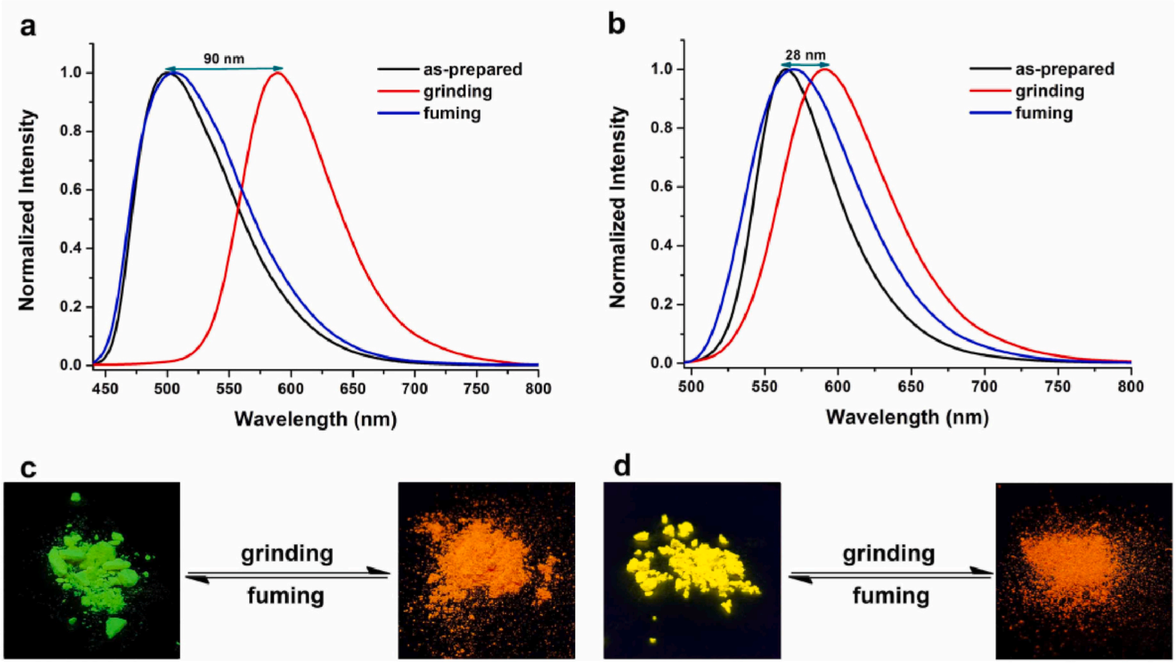

Fig. 4. The normalized PL spectra of different solids (as-prepared powder, ground powder, and fumed powder) for **PTZ-DPS** (a, $\lambda_{ex} = 420$ nm) and **BPTZ-DPS** (b, $\lambda_{ex} = 450$ nm). The fluorescence images of different solids for **PTZ-DPS** (c) and **BPTZ-DPS** (d) under 365 nm UV light.

transitions for the LE state, while the extreme weak emission in polar solvents is attributed to the fast interconversion from the emissive LE state to the low emissive ICT state.

The electrochemical properties of the target componds **PTZ-DPS** and **BPTZ-DPS** were investigated by cyclic voltammetry (CV) (Fig. S1). From the redox potential onset, we can calculate the HOMO and LUMO levels (Table S1). Both **PTZ-DPS** and **BPTZ-DPS** exhibit two reversible redox couples in the cathodic region. **PTZ-DPS** shows two cathodic redox processes at the potentials of −1.08 and −1.82 V (*vs.* Fc/Fc$^+$). For **BPTZ-DPS**, the two cathodic redox processes at a potential of −1.11 and −1.75 V (*vs.* Fc/Fc$^+$). By combination with the electron transition spectra, we can find that the LUMO energy levels of **PTZ-DPS** and **BPTZ-DPS** are −3.70 eV and −3.64 eV, and the HOMO energy levels are −6.34 eV and −6.26 eV, respectively (Table S1). In order to gain deeper insight into the effect of the geometric and electronic structures of **PTZ-DPS** and **BPTZ-DPS** on their photophysical properties, density functional theory (DFT) calculations were performed at the B3LYP/6-31G(d, p) level using Gaussian 09. The optimized molecular structures together with the frontier molecular orbital profiles that exhibit electronic distributions in their HOMO and LUMO are shown in Fig. 2 and Fig. 3, respectively. From Fig. 2, we can see clearly the optimized geometries of **PTZ-DPS** and **BPTZ-DPS** both display the V-shaped conformations with the bond angles of C–S–C as 109.9° and 106.1°, respectively. At the same time, the bowl-shaped conformation of phenothiazine unit in two compounds increases the warping degree of the whole molecule. Such strongly twisted molecular skeletons of **PTZ-DPS** and **BPTZ-DPS** can effectively prevent close packing and π-π interactions of molecules in the solid state. In other words, this leads to loose packing of molecules in the crystalline state, which probably endows the materials with obvious MFC behavior. As shown in Fig. 3, in each case, the HOMO orbital is concentrated predominantly on the phenothiazine units and the styrene moieties that connect with them, whereas the LUMO orbital is delocalized over diphenylsulfone segments together with the part of phenothiazine units. The shifts of electron densities of **PTZ-DPS** and **BPTZ-DPS** upon excitation imply the occurrence of ICT from the electron donor phenothiazine units to the electron acceptor diphenylsulfone moieties.

3.3. Mechanofluorochromic (MFC) properties

As discussed above, **PTZ-DPS** and **BPTZ-DPS** show similar emission performance in solutions. However, it can be seen that the emitting colors of the two compounds are significantly different from those of the as-prepared powders or the ground powders under UV illumination. Moreover, the emission switch could be obtained by repeating the treatment of mechanical grinding and fuming with DCM vapor. In order to investigate such solid emission properties that depend on the morphology and molecular structure, the PL spectra of **PTZ-DPS** and **BPTZ-DPS** in different solid states are measured. As shown in Fig. 4, upon illumination by 365 nm UV light, the as-prepared crystalline powders of **PTZ-DPS** and **BPTZ-DPS** could emit strong green and yellow light with the luminescence efficiencies as high as 32.84% and 39.69%, respectively. Meanwhile, the emission bands of the two as-prepared samples locate at 499 nm and 564 nm, respectively. After grinding by using a mortar and pestle, the as-prepared crystalline powders of the two compounds are transformed into ground powders. At the same time, the emission bands of as-prepared samples red shift to 589 nm and 592 nm (Fig. 3a and b), respectively, which implies that the grinding-induced large spectral red-shifts for the two luminophores are up to 90 nm and 28 nm, and the bright orange emitting ground solids with the slightly reduced luminescence efficiencies of 21.49% and 25.05% for both compounds are observed (Fig. 3c and d). The above test results fully indicate that **PTZ-DPS** and **BPTZ-DPS** have significant MFC nature. Interestingly, after the ground samples of the two compounds are placed in DCM vapor for 30 s, the orange emitting ground powders of **PTZ-DPS** and **BPTZ-DPS** could be transferred into green and yellow emitting solids that are similar to the as-prepared powders. Accordingly, their emission peaks return to positions that are almost the same as the ones of the initial powders. And when the fumed samples are re-ground, the same effectiveness as the first grinding are observed again. This illustrates that the MFC behavior of **PTZ-DPS** and **BPTZ-DPS** have good reversibility, and the reversible fluorescence color change could be repeated many times by alternate grinding and fuming cycles (Fig. S2) (see Fig. 5).

According to the above research results, both **PTZ-DPS** and **BPTZ-DPS** possess reversible stimuli-responsive fluorochromic properties, and

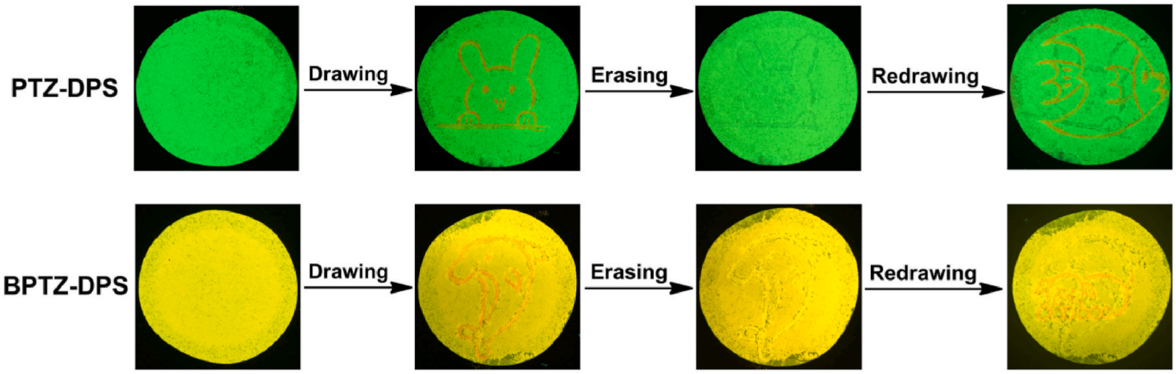

Fig. 5. Photographs of the drawing/erasing cycle for **PTZ-DPS** and **BPTZ-DPS** under 365 nm UV light lamp.

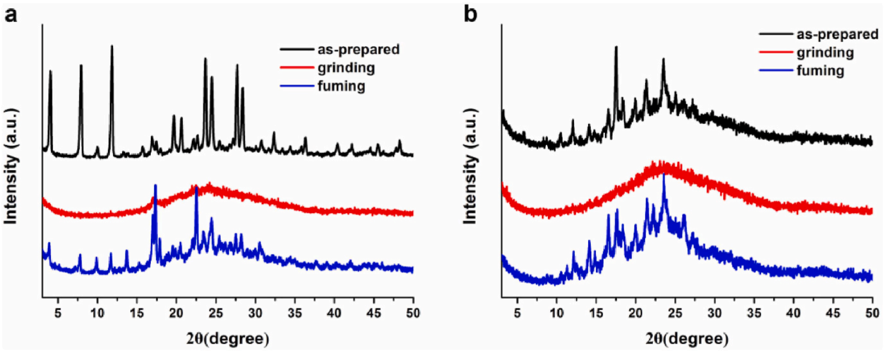

Fig. 6. PXRD patterns of **PTZ-DPS** (a) and **BPTZ-DPS** (b): as-prepared sample, ground sample, and fumed powders.

thus they become a kind of smart materials with the potential applications in optical storage, security papers, Anti-counterfeiting, etc. Therefore, we develop the simple, facile, and portable ink-free information storage paper. As shown in Fig. 5, after coating the solid powders of **PTZ-DPS** and **BPTZ-DPS** on the filter papers using their suspension in methanol, and the papers showing green and yellow fluorescence are obtained. When we draw a rabbit and a dolphin on the above papers with a glass rod directly, respectively, the clear patterns, which are maintained and can last for a month or more, are observed in orange fluorescence against the green and yellow backgrounds. Then, the rabbit and dolphin patterns can be erased quickly by exposing the drawing papers to the DCM vapor. In the next drawing, a fish and a pig with orange fluorescence (under UV lamp) are clearly revealed on the papers again, respectively.

To gain insights into the mechanism of the MFC behavior of **PTZ-DPS** and **BPTZ-DPS**, powder X-ray diffraction (PXRD) experiments were conducted on their samples at different solid states. As shown in Fig. 6, the PXRD patterns of as-prepared solids show sharp and intense reflections, which indicates that the molecules of the two compounds exist as well-ordered microcrystals in the solid powders. However, upon grinding, these sharp peaks disappear. This is because the ordered stacking of molecules in the crystalline states for the as-prepared samples is destroyed under the external force, resulting in the amorphous states. Moreover, when the ground powders of the two compounds are fumed in the DCM vapor for 1 min, the sharp and intense reflection patterns corresponding to the as-prepared samples appear again due to the recrystallization under this condition. Following grinding and fuming treatments, the luminescence of **PTZ-DPS** and **BPTZ-DPS** samples can transfer between bright orange-emitting color of the ground solids (amorphous) and strong green- and yellow-emitting colors of the as-prepared solids (crystalline), respectively, and thus the highly contrast emissive difference is observed. Therefore, photophysical and PXRD measurements reveal that the MFC behavior of **PTZ-DPS** and **BPTZ-DPS** originates from the reversible morphological transformation between the crystalline and amorphous phases.

In order to further obtain the fluorescence excited-state decay

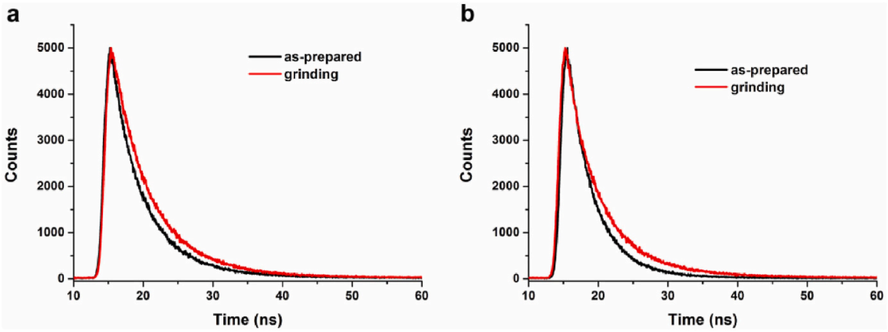

Fig. 7. Time-resolved emission-decay curves of **PTZ-DPS** (a) and **BPTZ-DPS** (b) solids before and after grinding.

Table 2
Fluorescence decay parameters of **PTZ-DPS** and **BPTZ-DPS** before and after grinding.

	Sample	τ_1 (ns)[a]	A_1[b]	τ_2 (ns)[a]	A_2[b]	$<\tau>$ (ns)[c]
PTZ-DPS	As-prepared	3.63	0.62	7.66	0.38	5.16
	Ground	4.40	0.59	8.54	0.41	6.10
BPTZ-DPS	As-prepared	3.04	0.68	5.63	0.32	3.87
	Ground	3.82	0.65	8.89	0.35	5.59

[a] Fluorescence lifetime.
[b] Fractional contribution.
[c] Weighted mean lifetime.

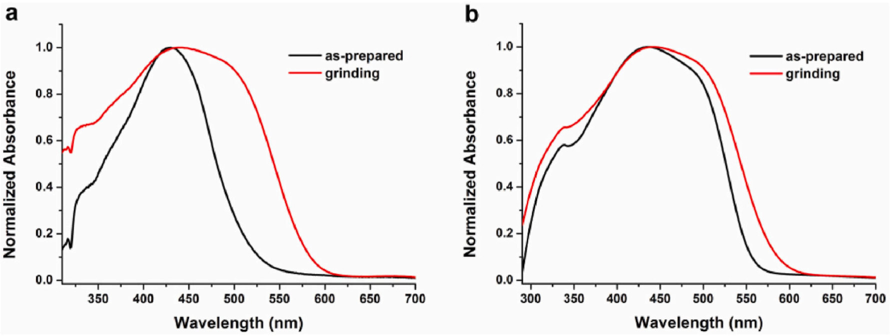

Fig. 8. Normalized solid UV–vis absorption spectra of **PTZ-DPS** (a) and **BPTZ-DPS** (b) in different solid states: as-prepared and ground.

information of **PTZ-DPS** and **BPTZ-DPS** solids before and after grinding, the fluorescence lifetimes are measured. The fluorescence decay curves of the two compounds are illustrated in Fig. 7. From Table 2, we can observe that there are two relaxation pathways for the as-prepared and ground solids of **PTZ-DPS** and **BPTZ-DPS** in their fluorescence decays, which suggests that the two compounds possess independent emissions from the segments with different π-conjugation lengths. The different pathways played different predominant roles for the solids before and after grinding. For **PTZ-DPS** and **BPTZ-DPS**, the excited molecules of the as-prepared powders mainly decay through the first pathway with the A_1 as 0.62 and 0.68, respectively. However, for their ground sample, the values of A_1 are 0.59 and 0.65, exhibiting an obvious difference. For the as-prepared solids of **PTZ-DPS** and **BPTZ-DPS**, the fluorescence lifetimes are estimated to be 5.16 ns and 3.87 ns, respectively, while the values increase to 6.10 ns and 5.59 ns for the ground sample. We believe that the change of molecular conformation and arrangements in their aggregation states is responsible for the change of fluorescence lifetimes [26].

It is well known that the release of the twist strain during the destruction of the crystalline structure will lead to the planarization of molecular conformation. And thus it will increase the molecular conjugation, resulting in the red-shift in the PL spectrum. In the case of **PTZ-DPS** and **BPTZ-DPS**, it is believed that the molecules of the two luminogens may adopt a more twisted conformation in order to fit into the crystalline lattice in their crystalline structures. When their crystalline structures are destroyed by mechanical force, the molecular conformation tends to be planar. This leads to the extension of the conjugated length of the molecule and subsequent planar intramolecular charge transfer (PICT) [10a,15a], and thus resulting in the obvious red shift of the emission bands. The above conclusion can be confirmed by comparing the absorption spectra of the powders before and after grinding. As shown in Fig. 8, upon grinding, the maximum absorption peaks of **PTZ-DPS** and **BPTZ-DPS** samples red shift from 430 nm to 436 nm–437 nm and 442 nm, respectively.

4. Conclusion

In summary, we have reported the design and synthesis of two D-A type luminescent switching materials **PTZ-DPS** and **BPTZ-DPS** based on the building units phenothiazine and electron-acceptor diphenylsulfone. The results show that the push-pull electronic structures and twisted molecular conformations not only endow **PTZ-DPS** and **BPTZ-DPS** with unique ICT behavior and intense fluorescence in both solution and solid state, but also enable them to possess good solid-state luminescence and remarkable and reversible stimulated fluorescence switching properties. Under stimulation of external force, the solid powders of **PTZ-DPS** and **BPTZ-DPS**, especially those of **PTZ-DPS**, exhibit the remarkable color change that is respectively from bright green and yellow to bright orange. Moreover, the color and emission intensities of **PTZ-DPS** and **BPTZ-DPS** can be switched by DCM vapors. PXRD study discloses that the force-induced phase transformation of the molecular packing from crystalline to amorphous states is response for the MFC behavior, and the obvious red-shifts of PL spectra upon grinding for the two luminophores come from the planarization of the molecular conformation and subsequent PICT. This study comprehensively reveals the origins of the stimuli-responsive luminescence properties of **PTZ-DPS** and **BPTZ-DPS**, and points out that they may be the candidates that can be applied to sensing, display devices with significant color-changing properties and other fields.

Author Statement

Zhou Hongke: Investigation, Formal analysis, Writing-Original draft preparation, Software. **Huang Qian:** Formal analysis, Data curation. **Liu Xingliang:** Visualization. **Xu Defang:** Methodology, Conceptualization, Investigation, Writing-Original draft preparation, Project administration. **Zhang Weidong:** Resources, Validation. **Fu Shengjie:** Writing-Reviewing and Editing. **Feng Xiucun:** Software. **Zhang Zhan:** Supervision.

Declaration of competing interest

The authors declare that they have no known competing financial interests or personal relationships that could have appeared to influence the work reported in this paper.

Acknowledgements

This work was financially supported by the National Natural Science Foundation of China (NNSFC, No. 21662028 and 21965031), the Project of Qinghai Science & Technology Department (Grant No. 2020-ZJ-923, 2018-HZ-817 and 2016-ZJY01), the Open Project of State Key Laboratory of Plateau Ecology and Agriculture, Qinghai University (Grant No. 2018-ZZ-4), and Qinghai Province “High-end Innovative Thousand

Talents Plan” (2017).

Appendix A. Supplementary data

Supplementary data to this article can be found online at https://doi.org/10.1016/j.dyepig.2020.108868.

References

[1] (a) Beyer MK, Clausen-Schaumann H. Mechanochemistry: the mechanical activation of covalent bonds. Chem Rev 2005;105:2921–48.(b) Chi Z, Zhang X, Xu B, Zhou X, Ma C, Zhang Y, et al. Recent advances in organic mechanofluorochromic materials. Chem Soc Rev 2012;41:3878–96. (c) Xue P, Ding J, Wang P, Lu R. Recent progress in the mechanochromism of phosphorescent organic molecules and metal complexes. J Mater Chem C 2016;4: 6688–706.(d) Luo X, Li J, Li C, Heng L, Dong YQ, Liu Z, et al. Reversible switching of the emission of diphenyldibenzofulvenes by thermal and mechanical stimuli. Adv Mater 2011;23:3261–5.

[2] (a) Lin W, Zhao Q, Sun H, Zhang KY, Yang H, Yu Q, et al. An electrochromic phosphorescent Iridium(III) complex for information recording, encryption, and decryption. Adv Opt Mater 2015;3:368–75.(b) Chen X, Sun G, Zhang T, Liu S, Zhao Q, Huang W. Utilization of electrochromically luminescent transition-metal complexes for erasable information recording and temperature-related information protection. Adv Mater 2016;28:7137–42.

[3] (a) Gong Y, He S, Li Y, Li Z, Liao Q, Gu Y, et al. Partially controlling molecular packing to achieve off–on mechanochromism through ingenious molecular design. Adv Optical Mater 2020:1902036.(b) Zhao J, Chi Z, Yang Z, Mao Z, Zhang Y, Ubba E, et al. Recent progress in the mechanofluorochromism of distyrylanthracene derivatives with aggregation-induced emission. Mater Chem Front 2018;2:1595–608.(c) Sagara Y, Mutai T, Yoshikawa I, Araki K. Material design for piezochromic luminescence: hydrogen-bond-directed assemblies of a pyrene derivative. J Am Chem Soc 2007;129:1520–1.(d) Yoshii R, Suenaga K, Tanaka K, Chujo Y. Mechanofluorochromic materials based on aggregation-induced emission-active boron ketoiminates: regulation of the direction of the emission color changes. Chem Eur J 2015;21:7231–7.

[4] (a) Sun H, Liu S, Lin W, Zhang KY, Lv W, Huang X, et al. Smart responsive phosphorescent materials for data recording and security protection. Nat Commun 2014;5:3601–9.(b) Kishimura A, Yamashita T, Yamaguchi K, Aida T. Rewritable phosphorescent paper by the control of competing kinetic and thermodynamic self-assembling events. Nat Mater 2005;4:546–9.(c) Fan G, Yang X, Liang R, Zhao J, Li S, Yan D. Molecular cocrystals of diphenyloxazole with tunable fluorescence, up-conversion emission and dielectric properties. CrystEngComm 2016;18:240–9.

[5] (a) Kumar P, Dwivedi J, Gupta B. Highly luminescent dual mode rare-earth nanorod assisted multi-stage excitable security ink for anticounterfeiting applications. J Mater Chem C 2014;2:10468–75.(b) He Z, Gao H, Zhang S, Zheng S, Wang Y, Zhao Z, et al. Achieving persistent, efficient, and robust room-temperature phosphorescence from pure organics for versatile applications. Adv Mater 2019:1807222.(c) Yang Z, Mao Z, Zhang X, Ou D, Mu Y, Zhang Y, et al. Intermolecular electronic coupling of organic units for efficient persistent room-temperature phosphorescence. Angew Chem Int Ed 2016;55:2181–5.

[6] (a) Xu B, Chi Z, Zhang J, Zhang X, Li H, Li X, et al. Piezofluorochromic and aggregation-induced-emission compounds containing triphenylethylene and tetraphenylethylene moieties. Chem Asian J 2011;6:1470–8.(b) Bu L, Sun M, Zhang D, Liu W, Wang Y, Zheng M, et al. Solid-state fluorescence properties and reversible piezochromic luminescence of aggregation-induced emission-active 9,10-bis[(9,9-dialkylfluorene-2-yl)vinyl] anthracenes. J Mater Chem C 2013;1: 2028–35.(c) Zhang Z, Yao D, Zhou T, Zhang H, Wang Y. Reversible piezo- and photochromic behaviors accompanied by emission color switching of two anthracene-containing organic molecules. Chem Commun 2011;47:7782–4.

[7] (a) Shen XY, Wang YJ, Zhao E, Yuan WZ, Liu Y, Lu P, et al. Effects of substitution with donor–acceptor groups on the properties of tetraphenylethene trimer: aggregation-induced emission, solvatochromism, and mechanochromism. J Phys Chem C 2013;117:7334–47.(b) Xu B, He J, Mu Y, Zhu Q, Wu S, Wang Y, et al. Very bright mechanoluminescence and remarkable mechanochromism using a tetraphenylethene derivative with aggregation-induced emission. Chem Sci 2015; 6:3236–41. (c) Sun T, Cheng D, Chai Y, Gong J, Sun M, Zhao F. High contrast mechanofluorochromic behavior of new tetraphenylethene-based Schiff base derivatives. Dyes Pigments 2019;170:107619.(d) Qi Q, Liu Y, Fang X, Zhang Y, Chen P, Wang Yi, et al. AIE (AIEE) and mechanofluorochromic performances of TPE-methoxylates: effects of single molecular conformations. RSC Adv 2013;3: 7996–8002.

[8] (a) Zhang Z, Xue P, Gong P, Zhang G, Peng J, Lu R. Mechanofluorochromic behaviors of β-iminoenolate boron complexes functionalized with carbazole. J Mater Chem C 2014;2:9543–51.(b) Zhou X, Li H, Chi Z, Zhang X, Zhang J, Xu B, et al. Piezofluorochromism and morphology of a new aggregation-induced emission compound derived from tetraphenylethylene and carbazole. New J Chem 2012;36:685–93.

[9] (a) Ying S, Chen M, Liu Z, Zheng M, Zhang H, Xue S, et al. Unusual mechanohypsochromic luminescence and unique bidirectional thermofluorochromism of long-alkylated simple DPP dyes. J Mater Chem C 2017;5: 5994–8.(b) Zhang K, Zhang Z, Fan X, Tang L, Ding Q, Yang K, et al. Enabling DPP derivatives to show multistate emission and developing the multifunctional materials by rational branching effect. Dyes Pigments 2018;159:290–7.

[10] (a) Zhang X, Chi Z, Xu B, Chen C, Zhou X, Zhang Y, et al. End-group effects of piezofluorochromic aggregation-induced enhanced emission compounds containing distyrylanthracene. J Mater Chem 2012;22:18505–13.(b) Dong Y, Zhang J, Tan X, Wang L, Chen J, Li B, et al. Multi-stimuli responsive fluorescence switching: the reversible piezochromism and protonation effect of a divinylanthracene derivative. J Mater Chem C 2013;1:7554–9.(c) Zhang X, Chi Z, Zhang J, Li H, Xu B, Li X, et al. Piezofluorochromic properties and mechanism of an aggregation-induced emission enhancement compound containing N-hexyl-phenothiazine and anthracene moieties. J Phys Chem B 2011;115:7606–11.

[11] Yoon S-J, Chung J, Gierschner J, Kim KS, Choi M-G, Kim D, et al. Multistimuli two-color luminescence switching via different slip-stacking of highly fluorescent molecular sheets. J Am Chem Soc 2010;132:13675–83.Kunzelman J, Kinami M, Crenshaw BR, Protasiewicz JD, Weder C. Oligo(*p*-phenylenevinylene)s as a “new” class of piezochromic fluorophores. Adv Mater 2008;20:119–22.

[12] Zhang Z, Wu Z, Sun J, Yao B, Xue P, Lu R. β-Iminoenolate boron complex with terminal triphenylamine exhibiting polymorphism and mechanofluorochromism. J Mater Chem C 2016;4:2854–61.Wang X, Liu Q, Yan H, Liu Z, Yao M, Zhang Q, et al. Piezochromic luminescence behavior of two new benzothiazole–enamido boron difluoride complexes: intra- and inter-molecular effects induced by hydrostatic compression. Chem Commun 2015;51:7497–500.(c) Fang W, Zhang Y, Zhang G, Kong L, Yang L, Yang J. Multi-stimuli-responsive fluorescence of a highly emissive difluoroboron complex in both solution and solid states. CrystEngComm 2017;19:1294–303.(d) Galer P, Korošec RC, Vidmar M, Šket B. Crystal structures and emission properties of the BF_2 complex 1-phenyl-3-(3,5-dimethoxyphenyl)-propane-1,3-dione: multiple chromisms, aggregation- or crystallization-induced emission, and the self-assembly effect. J Am Chem Soc 2014;136:7383–94.(e) Zhu J-Y, Li C-X, Chen P-Z, Ma Z, Zou B, Niu L-Y, Cui G, Yang Q-Z. A polymorphic fluorescent material with strong solid state emission and multi-stimuli-responsive properties. Mater Chem Front 2020;4:176–81.

[13] (a) Gao H, Xu D, Wang Y, Wang Y, Liu X, Han A, et al. Effects of alkyl chain length on aggregation-induced emission, self-assembly and mechanofluorochromism of tetraphenylethene modified multifunctional β-diketonate boron complexes. Dyes Pigments 2018;150:59–66.(b) Gao H, Xu D, Liu X, Han A, Zhou L, Zhang C, et al. Tetraphenylethene modified β-ketoiminate boron complexes bearing aggregation-induced emission and mechanofluorochromism. RSC Adv 2017;7:1348–56.(c) Gao H, Xu D, Wang Y, Zhang C, Yang Y, Liu X, et al. Aggregation-induced emission and mechanofluorochromism of tetraphenylbutadiene modified β-ketoiminate boron complexes. Dyes Pigments 2018;150:165–73.(d) Zhou L, Xu D, Gao H, Han A, Liu X, Zhang C, et al. Triphenylamine functionalized β-ketoiminate boron complex exhibiting aggregation-induced emission and mechanofluorochromism. Dyes Pigments 2017;137:200–7.

[14] (a) Mei J, Leung NLC, Kwok RTK, Lam JWY, Tang BZ. Aggregation-induced emission: together we shine, united we soar! Chem Rev 2015;115:11718–940.(b) Zhang D, Wen Y, Xiao Y, Yu G, Liu Y, Qian X. Bulky 4-tritylphenylethynyl substituted boradiazaindacene: pure red emission, relatively large Stokes shift and inhibition of self-quenching. Chem Commun 2008:4777–9.

[15] (a) Sun J, Dai Y, Ouyang M, Zhang Y, Zhan L, Zhang C. Unique torsional cruciform π-architectures composed of donor and acceptor axes exhibiting mechanochromic and electrochromic properties. J Mater Chem C 2015;3:3356–63.(b) Wang Y, Liu J, Yuan W, Wang Y, Zhou H, Liu X, et al. Unique twisted donor-acceptor cruciform π-architectures exhibiting aggregation-induced emission and stimuli-response behavior. Dyes Pigments 2019;167:135–42.(c) Xu D, Hao J, Gao H, Wang Y, Wang Y, Liu X, et al. Twisted donor–acceptor cruciform fluorophores exhibiting strong solid emission, efficient aggregation-induced emission and high contrast mechanofluorochromism. Dyes Pigments 2018;150:293–300.

[16] (a) Gong Y, Tan Y, Liu J, Lu P, Feng C, Yuan WZ, et al. Twisted D–π–A solid emitters: efficient emission and high contrast mechanochromism. Chem Commun 2013;49:4009–11.(b) Umar S, Jha AK, Purohit D, Goel A. A tetraphenylethene-naphthyridine-based AIEgen TPEN with dual mechanochromic and chemosensing properties. J Org Chem 2017;82:4766–73.

[17] (a) Jiang Y, Wang Y, Hua J, Tang J, Li B, Qian S, et al. Multibranched triarylamine end-capped triazines with aggregation-induced emission and large two-photon absorption cross-sections. Chem Commun 2010;46:4689–91.(b) Guo J, Li X-L, Nie H, Luo W, Gan S, Hu S, et al. Achieving high-performance nondoped OLEDs with extremely small efficiency roll-off by combining aggregation-induced emission and thermally activated delayed fluorescence. Adv Funct Mater 2017;27: 1606458.(c) Gong Y, Chen G, Peng Q, Yuan WZ, Xie Y, Li S, et al. Achieving persistent room temperature phosphorescence and remarkable mechanochromism from pure organic luminogens. Adv Mater 2015;27:6195–201.

[18] (a) Lu X, Xia M. Multi-stimuli response of a novel half-cut cruciform and its application as a security ink. J Mater Chem C 2016;4:9350–8.(b) Wang Y, Xu D, Gao H, Wang Y, Liu X, Han A, et al. Twisted donor–acceptor cruciform luminophores possessing substituent-dependent properties of aggregation-induced emission and mechanofluorochromism. J Phys Chem C 2018;122:2297–306.(c) Wang Y, Xu D, Gao H, Wang Y, Liu X, Han A, et al. Mechanofluorochromic properties of aggregation-induced emission-active tetraphenylethene-containing cruciform luminophores. Dyes Pigments 2018;156:291–8.

[19] Xue P, Yao B, Sun Xu Q, Chen P, Zhang Z, Lu R. Phenothiazine-based benzoxazole derivates exhibiting mechanochromic luminescence: the effect of a bromine atom. J Mater Chem C 2014;2:3942–50.

[20] Qiu X, Lu R, Zhou H, Zhang X, Xu T, Liu X, et al. Synthesis of linear monodisperse vinylene-linked phenothiazine oligomers. Tetrahedron Lett 2007;48:7582–5.

[21] Zhou H, Zhao X, Huang T, Lu R, Zhang H, Qi X, et al. Synthesis of star-shaped monodisperse oligo(9,9-di-n-octylfluorene-2,7-vinylene)s functionalized truxenes with two-photon absorption properties. Org Biomol Chem 2011;9:1600–7.

[22] Xie Z, Chen C, Xu S, Li J, Zhang Y, Liu S. White-light emission strategy of a single organic compound with aggregation-induced emission and delayed fluorescence properties. Angew Chem Int Ed 2015;54:7181–4.

[23] Liu X, Xu D, Lu R, Li B, Qian C, Xue P, et al. Luminescent organic 1D nanomaterials based on bis(β-diketone)carbazole derivatives. Chem Eur J 2011;17:1660–9.

[24] (a) Loiseau F, Campagna S, Hameurlaine A, Dehaen W. Dendrimers made of porphyrin cores and carbazole chromophores as peripheral units. Absorption spectra, luminescence properties, and oxidation behavior. J Am Chem Soc 2005;127:11352–63.(b) Xu T, Lu R, Liu X, Chen P, Qiu X, Zhao Y. Porphyrins with four monodisperse oligocarbazole arms: facile synthesis and photophysical properties. J Org Chem 2008;73:1809–17.

[25] (a) Xu D, Wang Y, Li L, Zhou H, Liu X. Aggregation-induced enhanced emission-type cruciform luminophore constructed by carbazole exhibiting mechanical force-induced luminescent enhancement and chromism. RSC Adv 2020;10:12025–34. (b) Lippert E, Naturforsch Z. Dipolmoment und Elektronenstruktur von angeregten Molekülen. A: Phys Sci 1955;10:541–5.(c) Mataga N, Kaifu Y, Koizumi M. Solvent effects upon fluorescence spectra and the dipolemoments of excited molecules. Bull Chem Soc Jpn 1956;29:465–70.

[26] Ongungal RM, Sivadas AP, Kumar NSS, Menon S, Das S. Self-assembly and mechanochromic luminescence switching of trifluoromethyl substituted 1,3,4-oxadiazole derivatives. J Mater Chem C 2016;4:9588–97.